Ladder-type electromagnetically induced transparency with optical pumping effect

Zong-Syun He, Jyh-Hung Tsai, Yung-Yung Chang, Chi-Chuan Liao, and Chin-Chun Tsai*
Department of Physics, National Cheng Kung University, Tainan 70101, Taiwan†
(Received 11 October 2012; published 4 March 2013)

This paper thoroughly elucidates the relative intensities of the probe transmission in a ladder-type electromagnetically induced transparency (EIT) system by considering the optical pumping effect. The observed EIT spectra reveal a different probe or coupling power dependence for various transmission peaks. In addition to causing quantum interference, the probe and coupling laser fields realign the population of Zeeman sublevels in the ground state through optical pumping. Analytical results indicate that the re-distribution levels, failing to contribute to the EIT peaks, either out of transition path or zero transition probability, significantly affect the transmission intensity.

DOI: 10.1103/PhysRevA.87.033402 PACS number(s): 32.80.Qk, 32.80.Xx, 32.70.−n

I. INTRODUCTION

Electromagnetically induced transparency (EIT) originates from two resonant laser fields coupled to a common state in a three-level system. EIT is a quantum interference effect in which a strong-coupling field results in the reduction in the absorption of a weak probe field. Among the many EIT-related applications in atomic physics and quantum optics, lasing without inversion [1], retrieval in both hot [2] and cold atoms [3], and all optical switches [4,5] are included. In atomic physics, EIT can explore the fine (hyperfine) structure of Rydberg states, owing to its narrow linewidth and high sensitivity [6–8]. However, the relative intensity of the transparency peaks under multi-intermediate levels of ladder-type EIT remains a task to be understood. Recent papers have examined the ladder-type EITs with optical pumping effect on different transitions called double-resonance optical pumping (DROP), which results from the population transferred to the other hyperfine states. The optical pumping effect occurs when a photon transfers its angular momentum to the atom, resulting in the orientation of atoms and population re-distribution in Zeeman sublevels. Investigations in the early 1950s discussed the interactions between circularly or linearly polarized light and atoms. Following atom-photon interactions, the distribution of atomic populations achieves a nonthermal equilibrium after several absorption-emission cycles. When the population prefers to implode in a certain Zeeman sublevel, this atomic system is generally assumed to be aligned or to be polarized. Such an atom is referred to as a polarized atom [9–11]. Investigations of relative intensity, concerning optical pumping for various transitions, have been focused on the population loss in the intermediate state [12], two-photon transition probability [12,13], and line shape of the EIT with DROP [14,15]. The method of multiphoton processes in a three-level atomic system was proposed as well [15,16]. The dispersionlike transmission spectrum has been experimentally observed [17] and has been theoretically modeled [18].

This paper investigates the three-level ladder-type EIT spectrum of Cs atoms in a vapor cell at room temperature. The transmission intensity of the EIT peaks as a function of the probe and coupling laser power is measured and is analyzed. The simulation spectrum of the two-photon transition probability in the coherence term ρ_{21} is integrated over the Boltzmann-Maxwell velocity distribution. The relative loss of population in sub-Zeeman levels due to the optical pumping effect is calculated as well. Finally, a quantitative result of the power dependence for the EIT transmission intensity is provided.

II. EXPERIMENTAL SETUP AND OBSERVATION

Figure 1 illustrates the energy levels for the D_2 line transitions of a cesium atom with fine (left) and hyperfine (right) structures. The frequency of weak probe and strong-coupling lasers correlates with the transitions of $|6\,^2S_{1/2}, F = 4\rangle \rightarrow |6\,^2P_{3/2}, F' = 4\rangle \rightarrow |11\,^2S_{1/2}, F'' = 4\rangle$ (the solid line is denoted as $44'4''$ for assignment). Under these experimental conditions, some other atoms with specific Doppler velocities resulting in resonance with the probe field can form two-photon Raman resonance EITs and can be observed while scanning the coupling frequency [19], such as the transition of $|6\,^2S_{1/2}, F = 4\rangle \rightarrow |6\,^2P_{3/2}, F' = 5\rangle \rightarrow |11\,^2S_{1/2}, F'' = 4\rangle$ (the dotted line is denoted as $45'4''$). In Fig. 1, the Rabi frequencies of probe and coupling transitions are Ω_p and Ω_c, and the decay rates of intermediate and final states are denoted as Γ_1 and Γ_2, which are 5.22 and 0.453 MHz, respectively [20]. The experiment in this paper is performed in a room-temperature atomic cesium cell with a length of 10 cm and an outer diameter of 2.54 cm as shown in Fig. 2. This cell is wrapped inside a shielding μ metal (three layers with an attenuation of 46 dB) to diminish the effect of the ambient magnetic field on the energy levels of Cs atoms. A linearly polarized probe field is provided by an external cavity diode laser (Sacher Lasertechnik Group TEC100, 100 mW), which produces a continuous wave (cw) at 852.3 nm. This laser frequency is locked on a Doppler-free saturation absorption spectrum on $|6\,^2S_{1/2}, F = 4\rangle \rightarrow |6\,^2P_{3/2}, F' = 4\rangle$ on which frequency uncertainty is determined to be approximately 0.53 MHz. The probe field passes through a linear polarizer before the cesium cell and a bandpass filter (852 nm, FWHM 10 nm) before a sensitive infrared detector (Electro-Optics Technology, Inc. ET-4000). The coupling field, as provided by a tunable cw dye laser (R6G dye, Coherent 899-21), tuned to around 574.6 nm, was expanded and was collimated into a beam diameter of 2.8 mm such that the probe field was covered and

*chintsai@mail.ncku.edu.tw
†http://www.phys.ncku.edu.tw/∼cctsai

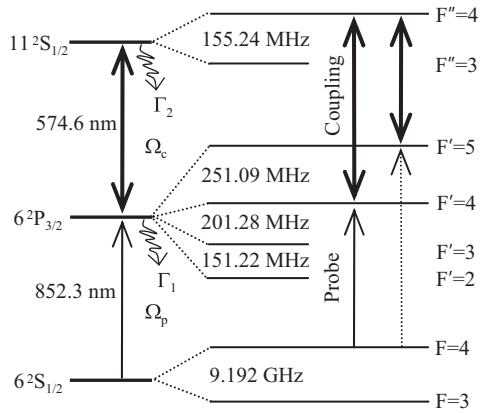

FIG. 1. Schematic energy levels of the cascade-type EIT of ^{133}Cs. Γ_1 and Γ_2 are the decay rate of the $6\,^2P_{3/2}$ state and the $11\,^2S_{1/2}$ state, and the Rabi frequencies of the probe and coupling transitions are Ω_p and Ω_c. The probe laser is frequency stabilized to the hyperfine transition of $|6\,^2S_{1/2}, F = 4\rangle \rightarrow |6\,^2P_{3/2}, F' = 4\rangle$, and the dotted line is the probe transition due to nonstationary atoms.

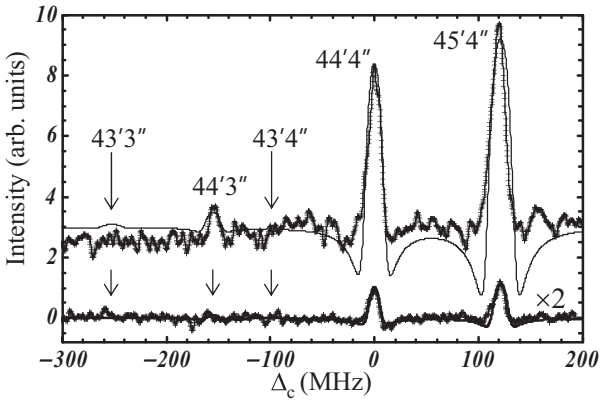

FIG. 3. Experimental spectra scanning the coupling frequency range around 500 MHz. The detuning Δ_c sets to zero for the on-resonance transition of $|6\,^2P_{3/2}, F' = 4\rangle \rightarrow |11\,^2S_{1/2}, F'' = 4\rangle$. The plus symbols denote the experimental data, and the solid line represents the simulation result. The arrows point out the possible EITs merged in the background. The top and lower traces are at different conditions of Ω_p and Ω_c.

was overlapped within the interaction region. These beams were counterpropagated through the cell to cancel the residual Doppler broadening [17]. The frequency of the coupling field was scanned across the $|6\,^2P_{3/2}, F' = 4\rangle \rightarrow |11\,^2S_{1/2}, F'' = 4\rangle$ transition by using the LABVIEW program. The probe field was intensity modulated by a mechanical chopper at around 1.0 kHz, which acted as the reference frequency for demodulation of a lock-in amplifier, and was recorded by a personal computer via a multiple interface card (National Instruments, MI/O 6035E). The power of the probe and coupling fields was varied by adding the neutral-density filters.

Figure 3 shows the Doppler-free EIT spectra as scanning the coupling frequency range around 500 MHz under a fixed probe laser frequency at $|6\,^2S_{1/2}, F = 4\rangle \rightarrow |6\,^2P_{3/2}, F' = 4\rangle$. The plus symbol denotes the experimental data, and the solid line represents the simulation result, which is discussed later. The detuning Δ_c sets to zero for on-resonance transition $|6\,^2P_{3/2}, F' = 4\rangle \rightarrow |11\,^2S_{1/2}, F'' = 4\rangle$. To illustrate the influence of the probe and coupling Rabi frequencies on the transition intensities, two different combinations of probe and coupling Rabi frequencies were used in Fig. 3; the top trace is at $\Omega_p = 1.72$ MHz (on the 45′ transition) and $\Omega_c = 19.65$ MHz

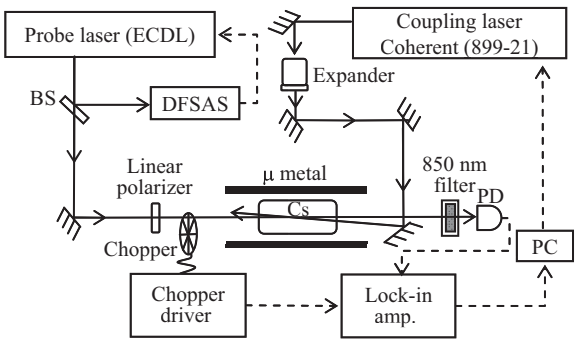

FIG. 2. Schematic of the experimental setup. BS: beam splitter; PD: photodetector associated with the transimpedance amplifier; lock-in amp.: lock-in amplifier; and PC: personal computer.

(on the 5′4″ transition), and the lower trace is at $\Omega_p = 0.804$ MHz (on the 45′ transition) and $\Omega_c = 12.07$ MHz (on the 5′4″ transition). The transitions of $|6\,^2S_{1/2}, F = 4\rangle \rightarrow |6\,^2P_{3/2}, F' = 4\rangle \rightarrow |11\,^2S_{1/2}, F'' = 3$ and $4\rangle$ labeled as 44′3″ and 44′4″ are the on-resonance EITs from the contribution of atoms with zero velocity. The other transitions result from two-photon Raman resonance EITs, which are originally from the contribution of nonstationary atoms with velocities of around +172 m/s for 43′3″ and 43′4″ and −214 m/s for 45′4″. These atoms interact as the resonance with the laser frequency of the $|6\,^2S_{1/2}, F = 4\rangle \rightarrow |6\,^2P_{3/2}, F' = 4\rangle$ transition by the Doppler shift. Since the probe and coupling fields have to interact on atoms with the same velocity group, a wavelength mismatching factor (λ_p/λ_c) has to be considered for the peak positions. The enhanced absorption dips on both wings of the EIT come from the residual Doppler effect due to wavelength mismatching between the probe and the coupling lasers, resulting from an imperfect two-photon Doppler-free phenomenon [21]. Details of the assignment can be found elsewhere [19]. The EITs of 43′3″ and 43′4″ (the arrows pointed) are hard to observe from the background, and the signal of 44′3″ has a signal-to-noise ratio about 1 under the capable Rabi frequency used in this experiment. Therefore, to investigate the transition intensity as a function of the probe and coupling Rabi frequencies, the transitions of 44′4″ and 45′4″ are focused. Figure 4 displays the recorded spectra of the transitions of 44′4″ and 45′4″ when varying the Rabi frequency of the (a) probe and (b) coupling laser fields. The Rabi frequency related to the transition probability (or strength) will significantly affect the EIT behavior [22]. For a given transition, the Rabi frequency is proportional to the square of the laser intensity [23] and is controlled experimentally by adjusting the laser power for a fixed laser-beam size. The spectra clearly reveal that the transparent intensity of the 44′4″ and 45′4″ peaks has a different growth and decline rate while adjusting the Rabi frequency of the probe and coupling fields. In Fig. 4(a), the spectra (vertically shifted from bottom to top traces) has the Rabi frequency of the

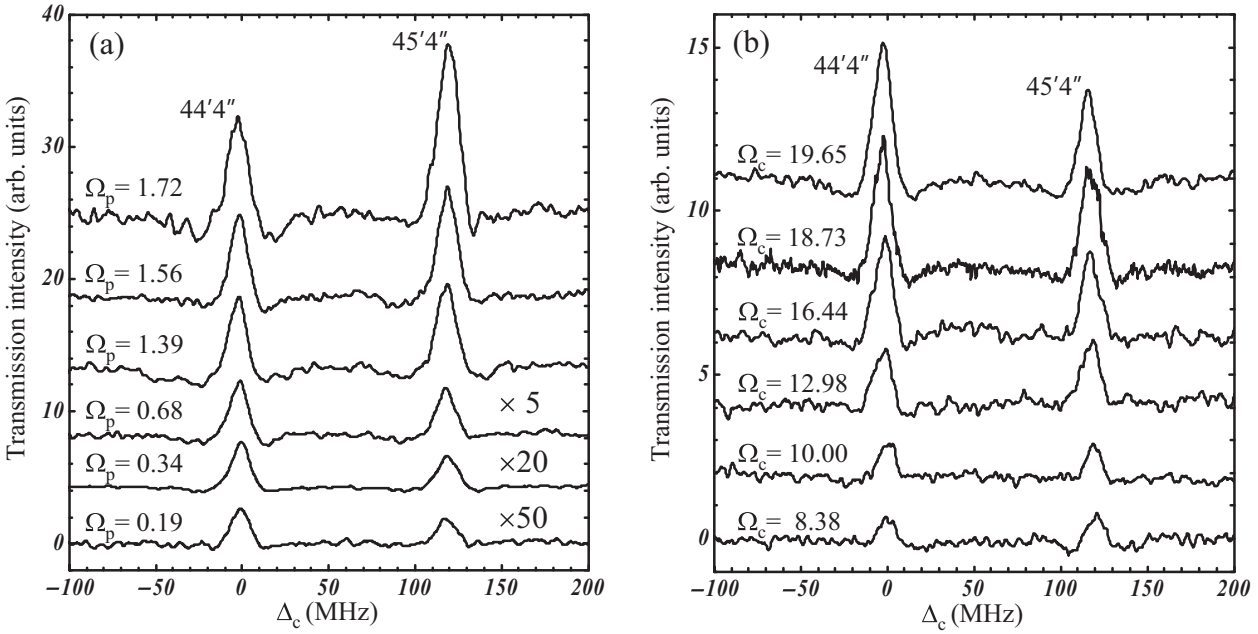

FIG. 4. Experimental spectra of the power dependence of (a) the probe and (b) the coupling fields as the scanning coupling frequency. The corresponding Rabi frequency in megahertz is listed near the trace. Ω_c is fixed at 16.06 MHz on the $5'4''$ transition in (a), and Ω_p is fixed at 0.80 MHz on the $45'$ transition in (b). The probe and coupling fields are both π-linearly polarized light. Frequency zero, corresponding to the $44'4''$ peak, is a transition of $|6\,^2S_{1/2}, F = 4\rangle \rightarrow |6\,^2P_{3/2}, F' = 4\rangle \rightarrow |11\,^2S_{1/2}, F'' = 4\rangle$.

probe field Ω_p on the $45'$ transition at 0.19, 0.34, 0.68, 1.39, 1.56, and 1.72 MHz, respectively, as the Rabi frequency of the coupling field Ω_c is fixed at 16.06 MHz on the $5'4''$ transition. The peak height ratio of $45'4''/44'4''$ increases when increasing the Rabi frequency of the probe field. In Fig. 4(b), the spectrum (vertically shifted from bottom to top traces) has the Rabi frequency of the coupling field Ω_c on the $5'4''$ transition at 8.38, 10.00, 12.98, 16.44, 18.73, and 19.65 MHz, respectively, as the Rabi frequency of the probe field Ω_p is fixed at 0.80 MHz on the $45'$ transition. This figure reveals that the peak height ratio for the transition intensity of $45'4''/44'4''$ gradually decreases when increasing the Rabi frequency of the coupling field. To understand the peak height ratio of the transitions of $45'4''/44'4''$, a simulation based on the theoretical model described in next section is presented.

III. THEORETICAL ANALYSIS

For a two-level atomic system, the radiation transmitted through the atoms is

$$I_t = I_0 e^{-(\alpha * l)}, \tag{1}$$

where l denotes the length of the atomic cell and α represents the absorption coefficient. Consider atoms with Doppler velocity distribution v along the laser beam at temperature T in which the absorption coefficient α must be integrated over all possible velocities and can be expressed as (consider the transition of $|6\,^2S_{1/2}, F = 4\rangle \rightarrow |6\,^2P_{3/2}, F' = 4\rangle$)

$$\alpha = n\frac{3\lambda^2}{2\pi}\frac{\Gamma_1}{\Omega_p}\frac{1}{\sqrt{\pi}u}\int_{-\infty}^{\infty} Im[\rho_{21}]e^{-(v/u)^2}dv, \tag{2}$$

where n is the atomic density, λ and Ω_p represent the wavelength and the Rabi frequency of the probe laser coupled to the lower transition, Γ_1 refers to the decay rate of the upper state, $u = (2k_BT/M)^{1/2}$ is the most probable speed (where k_B is the Boltzmann constant, and M is the atomic mass) [24], and ρ_{21} refers to the element of the density matrix derived from optical Bloch equations [25,26]. For a three-level ladder-type EIT (see Fig. 1), the matrix element ρ_{21} can be derived by solving the steady-state optical Bloch equations with first-order perturbation approximation under the weak probe field regime and can be written in the form

$$\rho_{21} = \frac{\Omega_p/2}{\Delta_p - i\frac{\Gamma_1}{2} - \frac{(\Omega_c/2)^2}{(\Delta_p+\Delta_c)-i\frac{\Gamma_2}{2}}}\rho_{11}, \tag{3}$$

where Δ_p and Δ_c denote the detuning of the probe and the coupling fields with respect to their atomic transition energies and ρ_{11} represents the probability of atoms being in the ground-state Zeeman sublevels [26]. In the density matrix, the diagonal elements are the probability of atoms being in a particular state, whereas, the off-diagonal elements refer to the coherence associated with the transitions. Generally speaking, ρ_{11} is set to 1 in a pure-state system, i.e., an ideal three-level system. However, if the system involves multiple energy levels, then ρ_{11} can be treated as the interaction probability of the population being in the transitions [27]. In this nonpure three-level system, the two-photon transition probability is the sum of all possible intermediate levels $m_{F'}$, $\sum_{m_F\rightarrow m_{F'}, m_{F'}\rightarrow m_{F''}}(|d_{m_F m_{F'}}|^2|d_{m_{F'} m_{F''}}|^2)$, where $d_{m_F m_{F'}}$ denotes the dipole matrix element between two Zeeman sublevels m_F and $m_{F'}$. Based on this factor, Moon *et al.* [12] explained the relative intensity of transmission for laser fields coupled with different transitions in the Rb atom, and McGloin *et al.* [13] proved experimentally that the greater the two-photon transition probability is, the greater the EIT

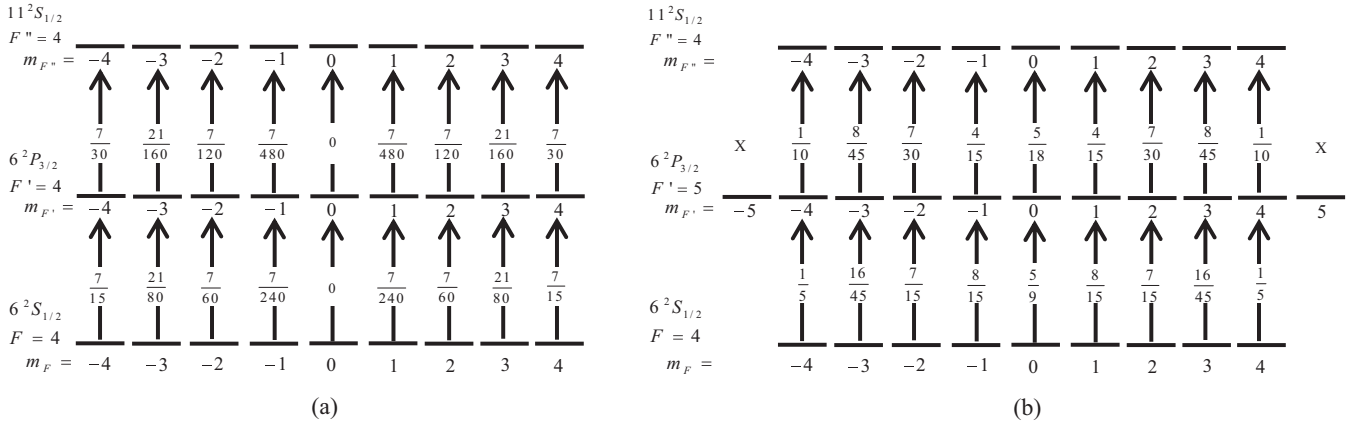

FIG. 5. Possible Zeeman-sublevel transition probabilities in the case of the π-π linearly polarized probe and coupling fields. (a) The $44'4''$ transition and (b) the $45'4''$ transition. The symbols X in (b) indicate no possible transition occurring in this case.

feature is. For the transitions involved in this experiment, the two-photon transition probabilities for $44'4''$ and $45'4''$ are 0.301 and 0.823, respectively, as applying π-π polarized fields, and the probabilities of the population being in the transition cycles have to be imported. Furthermore, the collision rate for the atoms at room temperature is significantly higher than those cold atoms in the trap. Collision-induced nonradiative energy transfer, which occurs in the dipole forbidden transitions, severely degrades the degree of quantum interference, especially at low-coupling Rabi frequency. The transmission of the probe field is not only affected by the Rabi frequency of the coupling field, but also by this nonradiative dephasing rate [22]. In general, this dephasing factor will broaden the transmission linewidth. Thus, a dephasing rate of 8 MHz, as derived from fitting the transmission linewidth, is included in the optical Bloch equations to handle the dipole forbidden transition between initial and final states [28].

Figure 5 shows the calculated transition probabilities for each Zeeman sublevel in the case of the π-π polarized probe and coupling fields on the (a) $44'4''$ transition and (b) $45'4''$ transition. These transition probabilities are derived by normalizing all of the decay channels of each hyperfine state [23]. According to Fig. 5(a), for the probability of transitions, in Zeeman sublevels, $m_F = 0$ to $m_{F'} = 0$ and $m_{F'} = 0$ to $m_{F''} = 0$ are zero, thus, $m_F = 0$ and $m_{F'} = 0$ make no contribution to the EIT signal and are called dark states. Correspondingly, the dark states due to the out-of-transition path are in the Zeeman sublevels of $|m_{F'}| = 5$ for the $45'4''$ transition shown in Fig. 5(b). For a lower transition of ladder-type EIT, the initial population distribution of ground-state Zeeman sublevels is in thermal equilibrium. However, the probe and coupling photons do not only interact with atoms to form an EIT, but also realign the atoms to a different population distribution. This realignment is owed to optical pumping in which the rate equations, including depopulation pumping, repopulation pumping, and relaxation rates in the steady state, must be solved to obtain the nonthermal equilibrium distribution. Franzen and Emslie [29] and Krainska-Misczak [11] provide further details for considering the optical pumping. When atoms are pumped into these dark states that are not involved in the interactions, i.e., population out of the transition strength or path, subsequently, decreases the EIT intensity.

In the ladder-type EIT, the optical pumping effect occurs both in the transitions of the ground state (i.e., the lower transition of the EIT) and the intermediate state (i.e., the upper transition of the EIT). For the lower transition, the initial distribution of the ground state is at thermal equilibrium in all of the Zeeman sublevels at room temperature. After solving the time-dependent differential rate equations for noncycling transition and taking the steady-state approach, the nonthermal equilibrium population redistribution of the ground state can be obtained and, hence, the interacting population ratio. Those populations in the dark state or out of transition make no contribution to the intensity of the EIT. Next, for the optical pumping in the intermediate state, the populations in the dark state or out of transition in the lower transition are removed, subsequently, allowing for the initial distribution of the upper transition. Correspondingly, the rate equations of the upper transition in the steady state can be solved again. Finally, the interaction population ratio of the upper transition is settled by normalizing at the initial population for the upper transition. Apparently, the product of the population ratios for the lower and upper transitions can be used as the optical pumping (O.P.) factors, implying that the population ratio remains in the ladder-type EIT transition and then contributes to the EIT intensity.

Table I lists the optical pumping results with some typical probe and coupling Rabi frequencies. The lower (upper) ratio refers to the population ratio involved in the interaction (not in the dark states or out-of-transition strength) on the lower (upper) transitions. By using π-polarized light, the optical pumping effect favors the population at the lower $|m_F|$ levels. For the $44'4''$ transition, the lower and upper ratios indicate the population ratios in magnetic sublevels in $F = 4$ and $F' = 4$ both, except for $m = 0$. As for the $45'4''$ transition, the lower ratio means the population ratio in magnetic sublevels in $F = 4$, and the upper ratio means the population ratio in magnetic sublevels in $F' = 5$, except for $|m| = 5$. With an increasing probe power due to faster absorption-emission cycles, more populations are pumped into the sublevel of $m_F = 0$. Therefore, in the $44'4''$ transition, less population is involved in the interactions since there is a dark state of the sublevel of $m_F = 0$. Hence, the lower ratio decreases with increasing the probe laser power. Consequently, for the $44'4''$ transition, the upper ratio does not vary too much since only a

TABLE I. The population ratios vary with some typical probe (upper part) and coupling (lower part) Rabi frequencies. The lower (upper) ratio refers to the population ratio involved in the interactions, which is not in the dark states on the lower (upper) transition. The O.P. factor is the product of the lower and upper ratios.

Transition	Ω_p (MHz)	Lower ratio (%)	Upper ratio (%)	O.P. (%)
$44'4''$	0.056	88.81	94.49	83.91
	0.176	88.02	94.27	82.98
	0.557	78.22	92.98	72.73
	1.243	47.82	91.85	43.92
$45'4''$	0.080	100	54.68	54.68
	0.254	100	57.19	57.19
	0.804	100	65.73	65.73
	1.799	100	69.47	69.47
Transition	Ω_c (MHz)	Lower ratio (%)	Upper ratio (%)	O.P. (%)
$44'4''$	3.91	78.22	99.31	77.68
	8.76	78.22	96.47	75.46
	12.39	78.22	92.83	72.62
	17.52	78.22	85.84	67.15
$45'4''$	5.13	100	98.02	98.02
	11.47	100	82.70	82.70
	16.22	100	65.15	65.15
	22.94	100	44.51	44.51

smaller amount of the population is pumped into the sublevel of $m_{F'} = 0$ after removing the population of $m_F = 0$. Consider the $45'4''$ transition; there is no dark state on the lower $45'4''$ transition. Although an optical pumping of the π-polarized probe field increases the population into the lower $|m_F|$ since they are all involved in the interactions, therefore, the lower ratio is 100%. Moreover, this distribution favors the lower $|m_F|$ levels, which prevents the upper optical pumping that pumps the populations into the dark state, i.e., sublevels $|m_{F'}| = 5$. When the population implodes into the lower $|m_{F'}|$ levels, more absorption-emission cycles are required to reach higher $|m_{F'}|$ levels. Therefore, the power dependence of the $45'4''$ transition relies more on the probe power. Similarly, the large upper ratio occurs on the weak-coupling power in the case of the power dependence of the coupling field. In Table I, the O.P. factor is the product of the lower and upper ratios. This factor indicates the ratio of populations involved in the ladder-type EIT transitions. The optical pumping effect may exist as another route to other ground states. For example, there exist other ground states $|6\,^2S_{1/2}, F = 3\rangle$ for the $44'$ transition, and $|6\,^2P_{3/2}, F' = 3$ and $4\rangle$ for the $5'4''$ transition, and so on. However, on average cycles, the product of the O.P. factor and the two-photon transition probability imports the total interaction population being in the transition, except for the quantity out of the transition strength and out of the cycles, to another hyperfine state. In other words, the matrix element ρ_{11} in Eq. (3) is effectively replaced with the product of the two-photon transition probabilities and the O.P. factor while considering the EIT applied in a nonpure three-level system, which is the existing dark states corresponding to certain polarization laser fields.

In the simulation, as for the transmission of Eq. (1), absorption coefficient α on the power of the exponential can be rewritten as $D_{RT}\frac{1}{l}\frac{\gamma}{\Omega_p}\int_{-\infty}^{\infty} Im[\rho_{21}]e^{-(v/u)^2}dv$, where $D_{RT} = n\frac{3\lambda^2}{2\pi}\frac{\Gamma_1}{\gamma}l\frac{1}{\sqrt{\pi}u}$ denotes the optical depth of an atomic cell at room temperature and γ represents the two-level absorption linewidth. In the steady-state condition of a two-level system with an on-resonance probe field and in the weak power regime, D_{RT} depends on ρ_{21} (for the two level system only). In the experiment, D_{RT} can be obtained by determining the pure two-level absorption of a D_2 line of cesium as the laser frequency lock on the $44'$ or $45'$ transitions, and γ can be determined by measuring the linewidth from a Doppler-free

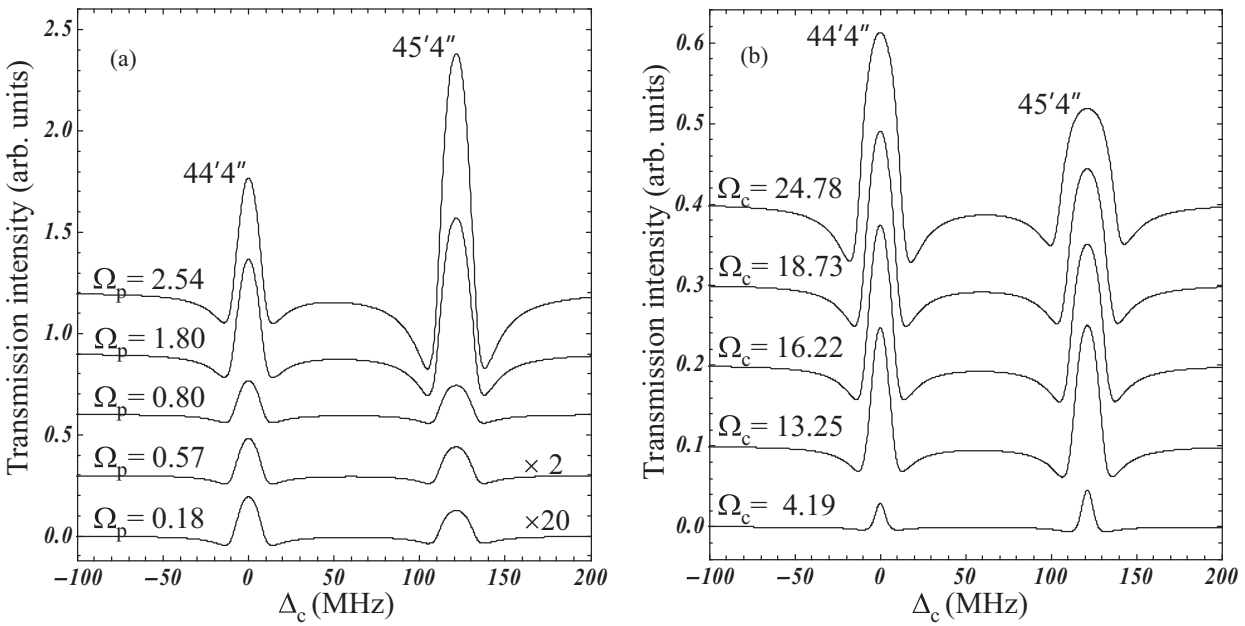

FIG. 6. Simulation spectra of a cascade EIT for a Cs atom by considering a two-photon transition probability and the O.P. factors. The case of (a) probe power dependence and (b) coupling power dependence. Ω_c is fixed at 16.06 MHz on the $5'4''$ transition in (a), and Ω_p is fixed at 0.804 MHz on the $45'$ transition in (b). All the units of Ω_p and Ω_c are in megahertz.

saturation spectroscopy [24]. The D_{RT} values and γ are 2.11 and 12.12 MHz for the $44'$ transition and are 3.02 and 8.46 MHz for the $45'$ transition under our experimental conditions.

Figure 6 summarizes the simulation spectra as mentioned earlier and considers the product of the two-photon transition probabilities and the O.P. factor as the influence of matrix element ρ_{11}, with respect to (a) the probe and (b) the coupling power dependence on the $44'4''$ and $45'4''$ transitions. Notably, the coherent term ρ_{21} in the density-matrix approach contains the higher-order terms, and integrated, it can deal with the power broadening and enhanced absorption in the EIT spectrum while considering the nonstationary atoms. The transmittance of the $44'4''$ and $45'4''$ peaks in Fig. 6 equals $I_t = I_0 e^{-(\alpha * l)}$, where $\alpha = D_{RT} \frac{1}{l} \frac{\gamma}{\Omega_p} \int_{-\infty}^{\infty} Im[\rho_{21}] e^{-(v/u)^2} dv$ and D_{RT} can be measured by Doppler-free saturation spectroscopy. The ρ_{11} term in the $Im[\rho_{21}]$ is replaced by two-photon transition probabilities and an O.P. factor in Table I for the corresponding Rabi frequency on the $44'4''$ and $45'4''$ transitions. With adjusting the power of (a) the probe and (b) the coupling fields, the spectra of the $44'4''$ and $45'4''$ transitions result in different situations of increasing rate, saturation conditions, broadening effects, and increasing absorption on the wings. According to Fig. 6(a), the Rabi frequencies of the probe field are 0.18, 0.57, 0.80, 1.80, and 2.54 MHz on the $45'$ transition for the vertically shifted spectrum from bottom to top traces as the Rabi frequency of the coupling field is fixed at 16.06 MHz on the $5'4''$ transition. This figure reveals that the linewidth broadening (i.e., saturation effect) [25] and the enhanced absorption on the wings of the EIT signals is gradually diminishing as the Rabi frequency of the probe field becomes comparable with the effective decay rate. The EIT phenomenon eventually ceases when an intensified probe field is applied, implying that the coherence quantum interference turns to decoherence; Raman absorption then dominates the interaction process [30]. Although the saturation effect can affect the transmission intensity, however, the optical pumping dominates the intensity of $44'4''$ eventually (as discussed later). According to Fig. 6(b), the Rabi frequencies of the coupling field are 4.19, 13.25, 16.22, 18.73, and 24.78 MHz on the $5'4''$ transition for the vertically shifted spectrum from bottom to top traces as the Rabi frequency of the probe field is maintained at 0.804 MHz on the $45'$ transition. The transmission linewidth becomes much broader, and the enhanced absorption on both wings of the EIT gets deeper while applying an intensified coupling field. And then, the Alter-Townes doublet dominates due to the saturation effect [22] (the power regime is not discussed in this paper). Correspondingly, when the Rabi frequency of the coupling field is comparable to the effective dephasing rate (8 MHz), the EIT signal fades out, that is, the probe field is less transparent as shown in the bottom lines of Fig. 6(b).

IV. RESULTS AND DISCUSSIONS

To avoid the normalization factor, this paper compares the ratios of the EIT peaks of transitions $45'4''$ to $44'4''$. Figure 7 illustrates the power dependence of (a) the probe and (b) the coupling fields for the experimental results (stars) with an error bar (standard deviation) and simulations (dashed and solid lines) of the ratio for the EIT peaks at transitions of $45'4''$ to $44'4''$. The dashed lines are the simulation results including the Doppler velocity group factor in integrating ρ_{21} of Eq. (2) due to the different EIT transitions as the frequency of the probe field is locked on the $44'$ transition and replacing the matrix element ρ_{11} with the two-photon transition probabilities only, i.e., without considering the depletion of the population out of the transition strength in the dark states. The solid lines are derived not only from including the Doppler velocity group factor in ρ_{21}, but also from replacing ρ_{11} with the product of the two-photon transition probabilities and the O.P. factor. The ratios of the solid lines can be obtained from Fig. 6. Apparently, the dashed lines are unable to explain the power dependence of the experimental intensity ratio. Since there is no adjustable parameter in the theoretical simulation, only with the O.P. factors included, the simulation results (solid lines) correlate well with the experimental observations in terms of the probe and coupling power dependence as shown in Fig. 7. According to Fig. 7(a), the ratio of transmission $45'4''/44'4''$ increases with the probe power. This increasing ratio originates from the loss interaction due to the populations in the dark state of

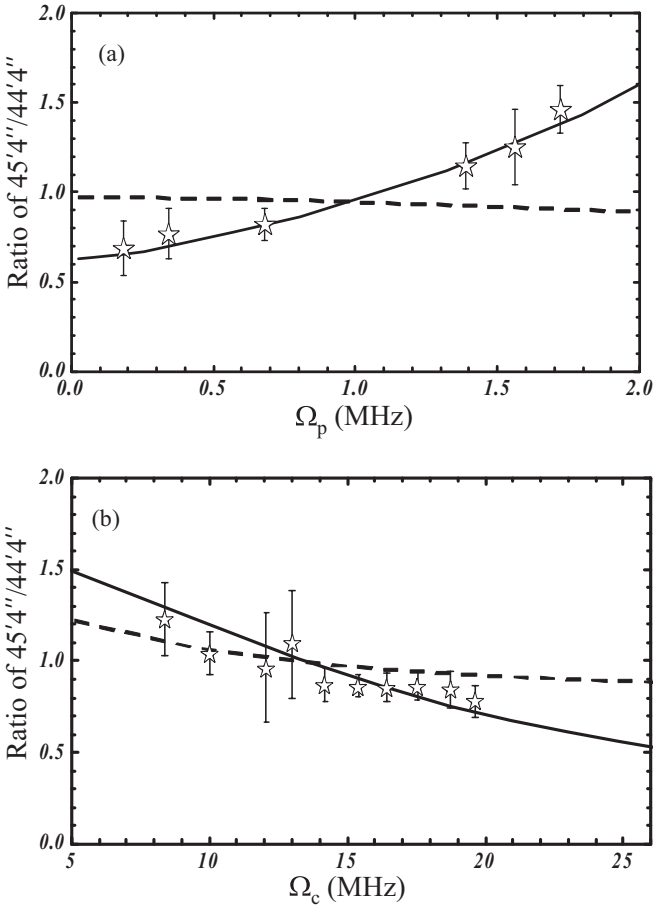

FIG. 7. The peak ratio of transmission $45'4''/44'4''$ as a function of (a) the probe and (b) the coupling Rabi frequencies for the $45'$ and $5'4''$ transitions, respectively. The star symbols are obtained from experimental results, and the solid line is the simulation result from Eqs. (1) and (2), considering the two-photon transition probability and the O.P. factors. The dashed line is the simulation result without the O.P. factors.

$m_F = 0$ for the $44'4''$ transition in the denominator. With an increasing power of the probe field, the population tends to implode on $m_F = 0$ and then out of the transition strength, subsequently, decreasing the transmittance. In contrast, this optical pumping effect favors the transition of $45'4''$ since it has a larger oscillator strength on lower $|m_F|$ levels and it requires more cycles to pump into the dark states of levels $|m_{F'}| = 5$ when the coupling power is fixed. The dashed line displays the saturation effect on transmission, causing the decreasing tendency that is attributed to the stronger transition strength on the $45'$ transition [25]. However, the optical pumping effect on the probe power dependence increases the ratio of $45'4''/44'4''$ eventually. According to Fig. 7(b), the ratio of $45'4''/44'4''$ tends to decrease with an increasing coupling power. This tendency is owed not only to the fact that the decreasing populations on $45'4''$ are faster than those on $44'4''$, but also to the saturation effect with an increasing coupling power. The larger error bars at the lower-coupling power are owed to the inability to observe the EIT spectrum when the Rabi frequency of the coupling field is nearly equal to or less than the dephasing rate of the upper transition [29,31]. The declining tendency on the dashed line displays the saturation effect without considering the optical pumping effect. The influence of the optical pumping on the power dependence is more direct on the probe field than that on the coupling field since the dark states on the upper transition require more absorption-emission cycles to reach the higher $|m_{F'}|$ levels. The optical pumping effect in the ladder-type EIT appears to be the major factor on the probe power dependence, yet it is not as severe on the coupling power dependence as shown by the dashed lines in Fig. 7. The mechanism of the ladder-type EIT fails to reach 100% transparency in a room-temperature cell, even when applied in a short cell [31]. In this case, there still always is absorption of the probe field. Consequently, the population in the intermediate state is observable but is not as much as that of the ground state on the lower transition. Therefore, the effect on coupling power dependence is not as correlated as that on the probe power. Despite a small portion of the population in the intermediate state, the O.P. factor is required to be considered with respect to coupling power dependence.

This paper investigates the transmission of EIT signals and qualitatively analyzes the optical pumping effects on populations in which the O.P. ratio and two-photon transition probability profoundly influence the relative transmission intensity. Additionally, the experimental value of D_{RT} and γ are incorporated in the calculation of the transmission to preclude the estimation of the constants in Eq. (2). Moreover, the transmission ratio of $45'4''/44'4''$ is used for modeling transmission intensity. We find that the optical pumping effect dominates the probe power dependence, and the effects on saturation and optical pumping are synergistic in the case of coupling power dependence by a using π-polarized light. The intensity of the EIT is primarily affected by the Rabi frequency, the optical pumping branch ratio, collisions between atoms, and as many other factors that were not taken into consideration. Even so, this simplified model is feasible in the weak power dependence on the EIT peaks' ratio.

ACKNOWLEDGMENTS

Z.-S. He would like to thank Professor Y.-F. Chen for his valuable suggestions. This research was supported by the National Science Council, Taiwan.

[1] S. E. Harris, Phys. Rev. Lett. **62**, 1033 (1989).
[2] D. F. Phillips, A. Fleischhauer, A. Mair, R. L. Walsworth, and M. D. Lukin, Phys. Rev. Lett. **86**, 783 (2001).
[3] C. Liu, Z. Dutton, C. H. Behroozi, and L. V. Hau, Nature (London) **409**, 490 (2001).
[4] S. E. Harris and Y. Yamamoto, Phys. Rev. Lett. **81**, 3611 (1998).
[5] M. Yan, E. G. Rickey, and Y. Zhu, Phys. Rev. A **64**, 041801 (2001).
[6] A. K. Mohapatra, T. R. Jackson, and C. S. Adams, Phys. Rev. Lett. **98**, 113003 (2007).
[7] M. Mack, F. Karlewski, H. Hattermann, S. Höckh, F. Jessen, D. Cano, and J. Fortágh, Phys. Rev. A **83**, 052515 (2011).
[8] A. Krishna, K. Pandey, A. Wasan, and V. Natarajan, Europhys. Lett. **72**, 221 (2005).
[9] W. B. Hawkins and R. H. Dicke, Phys. Rev. **91**, 1008 (1953).
[10] W. Happer, Rev. Mod. Phys. **44**, 169 (1972).
[11] M. Krainska-Miszczak, J. Phys. B **12**, 555 (1979).
[12] H. S. Moon, L. Lee, and J. B. Kim, J. Opt. Soc. Am. B **24**, 2157 (2007).
[13] D. McGloin, M. H. Dunn, and D. J. Fulton, Phys. Rev. A **62**, 053802 (2000).
[14] H. S. Moon, L. Lee, and J. B. Kim, Opt. Express **16**, 12163 (2008).
[15] H. S. Moon and H. R. Noh, Phys. Rev. A **84**, 033821 (2011).
[16] H. R. Noh and H. S. Moon, Phys. Rev. A **84**, 053827 (2011).
[17] B. Yang, J. Gao, T. Zhang, and J. Wang, Phys. Rev. A **83**, 013818 (2011).
[18] H. R. Noh and H. S. Moon, Phys. Rev. A **85**, 033817 (2012).
[19] Z. S. He, J. H. Tsai, M. T. Lee, Y. Y. Chang, C. C. Tsai, and T. J. Whang, J. Phys. Soc. Jpn. **81**, 124302 (2012).
[20] D. DiBerardino, C. E. Tanner, and A. Sieradzan, Phys. Rev. A **57**, 4204 (1998).
[21] S. Shepherd, D. J. Fulton, and M. H. Dunn, Phys. Rev. A **54**, 5394 (1996).
[22] Y. Q. Li and M. Xiao, Phys. Rev. A **51**, 4959 (1995).
[23] P. M. Farrell and W. R. MacGillivray, J. Phys. A **28**, 209 (1995).
[24] C. J. Foot, *Atomic Physics* (Oxford University Press, Oxford, 2005).
[25] H. R. Noh and H. S. Moon, Phys. Rev. A **80**, 022509 (2009).
[26] J. Gea-Banacloche, Y. Q. Li, S. Z. Jin, and M. Xiao, Phys. Rev. A **51**, 576 (1995).
[27] M. O. Scully and M. S. Zubairy, *Quantum Optics* (Cambridge University Press, Cambridge, UK, 1997).
[28] D. J. Fulton, S. Shepherd, R. R. Moseley, B. D. Sinclair, and M. H. Dunn, Phys. Rev. A **52**, 2302 (1995).
[29] W. Franzen and A. G. Emslie, Phys. Rev. **108**, 1453 (1957).
[30] R. Y. Chang, Y. C. Lee, W. C. Fang, M. T. Lee, Z. S. He, B. C. Ke, and C. C. Tsai, J. Opt. Soc. Am. B **27**, 85 (2010).
[31] R. R. Moseley, S. Shepherd, D. J. Fulton, B. D. Sinclair, and M. H. Dunn, Opt. Commun. **119**, 61 (1995).